

## Bose Polaron Interactions in a Cavity-Coupled Monolayer Semiconductor

Li Bing Tan,<sup>1,\*</sup> Oriana K. Diessel,<sup>2,\*</sup> Alexander Popert,<sup>1</sup> Richard Schmidt,<sup>3,†</sup> Atac Imamoglu,<sup>1,‡</sup> and Martin Kroner<sup>1,§</sup>

<sup>1</sup>*Institute for Quantum Electronics, ETH Zürich, CH-8093 Zürich, Switzerland*

<sup>2</sup>*Max-Planck-Institute of Quantum Optics, 85748 Garching, Germany*

<sup>3</sup>*Institute for Theoretical Physics, Heidelberg University, 69120 Heidelberg, Germany*



(Received 14 February 2023; accepted 3 August 2023; published 26 September 2023)

The interaction between a mobile quantum impurity and a bosonic bath leads to the formation of quasiparticles, termed Bose polarons. The elementary properties of Bose polarons, such as their mutual interactions, can differ drastically from those of the bare impurities. Here, we explore Bose polaron physics in a two-dimensional nonequilibrium setting by injecting  $\sigma^-$  polarized exciton-polariton impurities into a bath of coherent  $\sigma^+$  polarized polaritons generated by resonant laser excitation of monolayer MoSe<sub>2</sub> embedded in an optical cavity. By exploiting a biexciton Feshbach resonance between the impurity and the bath polaritons, we tune the interacting system to the strong-coupling regime and demonstrate the coexistence of two new quasiparticle branches. Using time-resolved pump-probe measurements, we observe how polaron dressing modifies the interaction between impurity polaritons. Remarkably, we find that the interactions between high-energy polaron quasiparticles, which are repulsive for small bath occupancy, can become attractive in the strong impurity-bath coupling regime. Our experiments provide the first direct measurement of Bose polaron-polaron interaction strength in any physical system and pave the way for exploration and control of many-body correlations in driven-dissipative settings.

DOI: [10.1103/PhysRevX.13.031036](https://doi.org/10.1103/PhysRevX.13.031036)

Subject Areas: Condensed Matter Physics, Photonics,  
Quantum Physics

### I. INTRODUCTION

Interactions between quasiparticles play a key role across condensed matter physics, determining novel phases of matter and governing the quantum dynamics of many-body systems. A paradigm for the physics of quasiparticles includes polarons arising from the interaction between a mobile impurity and a bath with a large number of degrees of freedom. The concept of polarons has been vital to develop effective descriptions of complex systems in terms of quasiparticles with properties such as an effective mass or lifetime that are modified compared to the bare impurity. Superconductivity provides a spectacular example for how polaron-polaron interactions could drastically deviate from those of the bare impurities: Here, electronic quasiparticles form bound Cooper pairs due to bath-mediated attraction even though bare impurities (the electrons) are subject to

repulsive Coulomb interactions. Recent experimental investigation of single atomic impurities interacting with degenerate Fermi or Bose gases of ultracold atoms demonstrated the formation of Fermi or Bose polarons [1–4]. The impurity-bath interaction in ultracold atomic systems can be tuned using Feshbach resonances, allowing one to enter the strong-coupling regime where the impurity energy and lifetime are drastically altered [5–7]. Recently, Fermi polarons were realized for the first time in solid-state physics where their formation explains the optical excitation spectrum of doped monolayer semiconductors [8].

An outstanding challenge in both the atomic and solid-state settings is to achieve a general understanding of how polaron quasiparticles interact with each other [9–12]. Importantly, an open question remains as to whether interactions between polarons in these settings can fundamentally alter the character of quasiparticle interactions from repulsive to attractive as an emergent feature of the many-body character of the system. This question becomes of particular interest as it now becomes experimentally possible to enter the strong-coupling regime where the interplay of exchange of low-energy excitations and the formation of a dressing cloud around each impurity can lead to strong nonperturbative effects.

In this article, we show that, based on a mechanism of strong-coupling Bose polaron polariton formation, the interactions between fundamentally repulsive exciton-polariton

\*These two authors contributed equally to this work.

†richard.schmidt@thphys.uni-heidelberg.de

‡imamoglu@phys.ethz.ch

§mkroner@phys.ethz.ch

quantum impurities in atomically thin semiconductors can not only be weakened but that the sign of interactions even be reversed. Our observation demonstrates how Bose polaron formation can be exploited as a means to control interactions, opening avenues towards new unconventional mechanisms of induced pairing in van der Waals materials based on exciton or polaron exchange. Our observations are consistent with Bose polaron theory extended to the description of a finite polaron density, where polaron formation acts as a mechanism to mediate attractive interactions. Remarkably, we find that the dissipative nature of excitons plays only a subleading role in the theoretical predictions, revealing the universal nature of the mechanism of exciton-mediated attraction.

Our work goes beyond the pioneering results reporting modified polariton-polariton interactions in the presence of a biexciton resonance that were obtained on conventional semiconductor quantum wells strongly coupled to microcavities, such as ZnSe [13] or GaAs [14,15]. Particularly, the latter experiment [15] used short pulses simultaneously exciting both upper and lower polariton branches. In Ref. [15], the hybridization of a collective excitation of biexcitons with the exciton and cavity modes is addressed, the precursor for the observation of the biexciton Feshbach resonance which was later reported in Ref. [16]. However, in all these reports, only impurity-bath interactions were studied, while here we report on the first measurement of impurity-impurity interactions and their modifications by the bath. In our experiments, we make use of the strong light-matter coupling to ensure that the pump pulse only generates lower polaritons.

## II. EXPERIMENTAL SCHEME

Our experiments are based on time-resolved pump-probe spectroscopy of exciton-polaritons created in a monolayer transition metal dichalcogenide that is strongly coupled to an optical microcavity. The pump generates a coherent state of lower exciton-polaritons of a large occupation number. These particles act as a quantum bath for the following probe pulse that generates a controllable density of exciton-polariton quantum impurities with a different valley quantum number. In the absence of the bath, these probe exciton-polaritons interact repulsively.

Upon switching on interactions between the pump and probe exciton-polaritons using a biexciton Feshbach resonance, we observe that the dressing of the probe exciton-polaritons leads to the formation of repulsive (RP) and attractive (AP) Bose polarons previously observed in ultracold atomic systems [5,7,17]. In our solid-state setting, we go beyond these previous studies where impurities were extremely dilute and enter the regime of finite polaron density. This reveals that the dynamical dressing of exciton-polaritons leads not only to smaller repulsive interactions between the higher-energy RP quasiparticles, but—by pushing the interspecies exciton interactions to the

strong-coupling limit—the sign of the interactions can be fully reversed.

Figure 1(a) shows a sketch of the device we studied where a monolayer of molybdenum diselenide ( $\text{MoSe}_2$ ) is embedded inside a zero-dimensional (0D) fiber cavity [8,11]. The  $\text{MoSe}_2$  is encapsulated between two hexagonal boron nitride (hBN) layers, where the bottom layer serves as a dielectric spacer that separates the  $\text{MoSe}_2$  from a graphene gate (Fig. 5 in the Appendix). Furthermore, it ensures that the graphene gate at the node and the  $\text{MoSe}_2$  at the antinode of the cavity electric field. The graphene and  $\text{MoSe}_2$  are each contacted separately using metal electrodes made of gold and titanium (Fig. 5 in the Appendix). A gate voltage  $V$  is applied to operate the device in the charge-neutrality regime of the  $\text{MoSe}_2$  monolayer. The heterostructure is deposited on a fused silica substrate whose surface is coated with a distributed Bragg reflector (DBR) mirror. The cavity is completed by a DBR-coated optical fiber facet with a concave dimple fabricated on the core (see the Appendix for details).

The elementary excitations of this coupled system are exciton-polaritons, whose properties we investigate at liquid helium temperatures [8,11]. In Fig. 1(b), we show the normalized transmission spectrum of the upper and lower exciton-polaritons of energy  $\omega_{\text{UP}}$  and  $\omega_{\text{LP}}$ , respectively, as a function of the voltage applied to the piezoelectric positioner that controls the cavity length and thereby the energy of the cavity mode  $\omega_{\text{C}}$ . The two excitonic species belonging to the K and K' valleys can be individually addressed by  $\sigma^-$ - and  $\sigma^+$ -polarized light. They are degenerate in the absence of a magnetic field and hence exhibit the same transmission spectrum when probed by a low-intensity continuous wave (cw) white light source. We exclusively study excitations of the lower branch in our experiments. Consequently, we use the term polariton to denote lower exciton-polaritons.

To investigate Bose polaron physics, we exploit the existence of a polariton Feshbach resonance between polaritons with opposite chirality, previously demonstrated in GaAs quantum wells embedded in a monolithic 2D DBR cavity [16]. In contrast to this prior experiment, we use a 0D cavity. We emphasise that despite the 0D nature of the cavity modes, LPs with momenta  $q \gg \omega_{\text{C}}/c$  experience continuous 2D dispersion, with  $c$  denoting the speed of light. Biexciton formation between two LPs with opposite polarization leads to a virtual excitation of high-momentum LPs with  $q \leq 1/a_{\text{XX}}$ , where  $a_{\text{XX}} \sim 2$  nm is the biexciton (Bohr) radius. Consequently, the virtually excited LP states that contribute to interactions are essentially excitonlike and are subject to a 2D dispersion relation. Since the contribution of discrete polariton modes to the overall impurity-bath interaction strength is negligible, a model for mobile quantum impurities (and a mobile bath) applies [18].

We resonantly excite the system with a narrow band ( $\leq 0.5$  meV, corresponding to  $\Delta t_{\sigma^+} \sim 3$  ps pulse length),

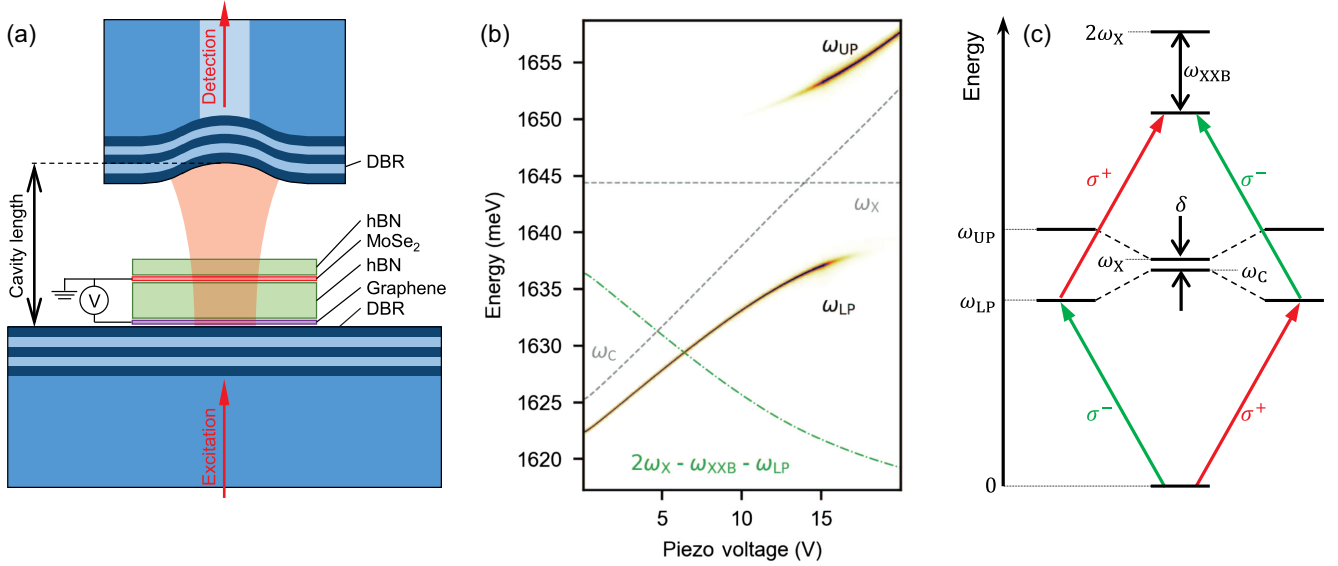


FIG. 1. (a) Schematic of the device structure. The semiconductor cavity consists of a van der Waals heterostructure deposited on a distributed Bragg reflector (DBR)-coated fused silica substrate. The substrate, along with a DBR-coated fiber with a concave facet on the core, forms a 0D cavity. The heterostructure consists of a molybdenum diselenide ( $\text{MoSe}_2$ ) monolayer (red) encapsulated by hexagonal boron nitride (hBN) layers (light green) and a graphene layer (purple) which acts as a gate. We excite the system through the substrate and collect the transmitted light through the fiber. (b) Transmission spectrum of the exciton-polaritons as a function of piezo voltage controlling the cavity detuning  $\delta = \omega_C - \omega_X$ , measured with a broad band cw white light source. For illustration purposes, the maximum intensity of the spectrum is normalized to 1 for each piezo voltage. The bare exciton energy  $\omega_X$  and the cavity energy  $\omega_C$  are indicated by gray dashed lines. The biexciton resonance condition for a polariton in one valley in the presence of a polariton in the other is shown by the green dash-dotted line. The red dashed box indicates the detuning range around the resonance condition  $2\omega_{LP} = 2\omega_X - \omega_{XXB}$ , which is examined using pump-probe spectroscopy. (c) Energy-level diagram to illustrate the experimental scheme. A K-valley polariton bath is resonantly created with a  $\sigma^+$ -polarized (pump) laser field (red arrow). The presence of this population allows for a resonant creation of a  $K'$ -valley polariton impurity population using a  $\sigma^-$ -polarized (probe) laser field (green arrow) to form a biexciton state.

strong  $\sigma^+$ -polarized pump pulse creating a bath of exciton-polaritons in the K valley (of density  $n_b$ ). We then measure the transmission spectrum of the  $K'$  impurity exciton-polaritons (of density  $n_i$ ) with a weak  $\sigma^-$ -polarized 7-meV broadband pulse ( $\Delta t_{\sigma^-} \sim 200$  fs). The time delay  $\tau$  between the pump pulse and the probe pulse, defined as the time difference between the arrival time of the peak of the probe pulse and the pump pulse, can be varied in our experiment (see the Appendix). Figure 1(c) shows the relevant energy states addressed in our experiment. In  $\text{MoSe}_2$ , two exciton-polaritons with opposite circular polarization (spin) can form a biexciton bound state of binding energy  $\omega_{XXB}$  below the two-exciton threshold at  $2\omega_X$  [19]. The green dash-dotted line in Fig. 1(b) shows the resonance condition  $\omega_{LP,\sigma^+} + \omega_{LP,\sigma^-} = 2\omega_X - \omega_{XXB}$  between the pump (bath) and probe (impurity) polariton energies with the biexciton energy as a function of the cavity detuning. Here, we use  $\omega_{XXB} = 29$  meV, obtained by recent ac-Stark shift measurements on bare  $\text{MoSe}_2$  excitons [20,21].

### III. BOSE POLARON FORMATION

The left panel of Figs. 2(a)–2(c) shows the normalized probe transmission spectrum as a function of time delay

when the polariton is tuned to 16.3, 15.5, and 14.6 meV below the exciton energy, respectively. At negative time delays  $\tau < -2$  ps, the probe population is generated in the sample before the bath population. As expected, the transmission remains peaked at the polariton energy. Starting from  $\tau = -2$  ps, the temporal overlap between the bath and probe population becomes significant and increases towards positive time delays. It is in this regime that we observe a clear modification of the transmission spectrum. At fixed detuning  $\omega_{LP} - \omega_X = -16.3$  meV [Fig. 2(a)], the peak of the transmission spectrum begins to redshift, and its magnitude becomes largest at around  $\tau = 2$  ps before relaxing back to the initial polariton energy. When the sum of the energy of bath and impurity polaritons equals  $2\omega_X - \omega_{XXB}$  [Fig. 2(b)], the transmission splits into two distinct peaks at zero delay, which persists until around  $\tau = 4$  ps. In contrast, for  $\omega_{LP} - \omega_X = -14.6$  meV [Fig. 2(c)], the peak of the transmission blueshifts for  $|\tau| \leq 4$  ps.

Figure 2(d) shows the normalized transmission spectrum (at  $\tau = 0$ ) obtained as a function of detuning and expressed with respect to the energy of the polariton impurity in the absence of the bath (at  $\tau = -50$  ps).

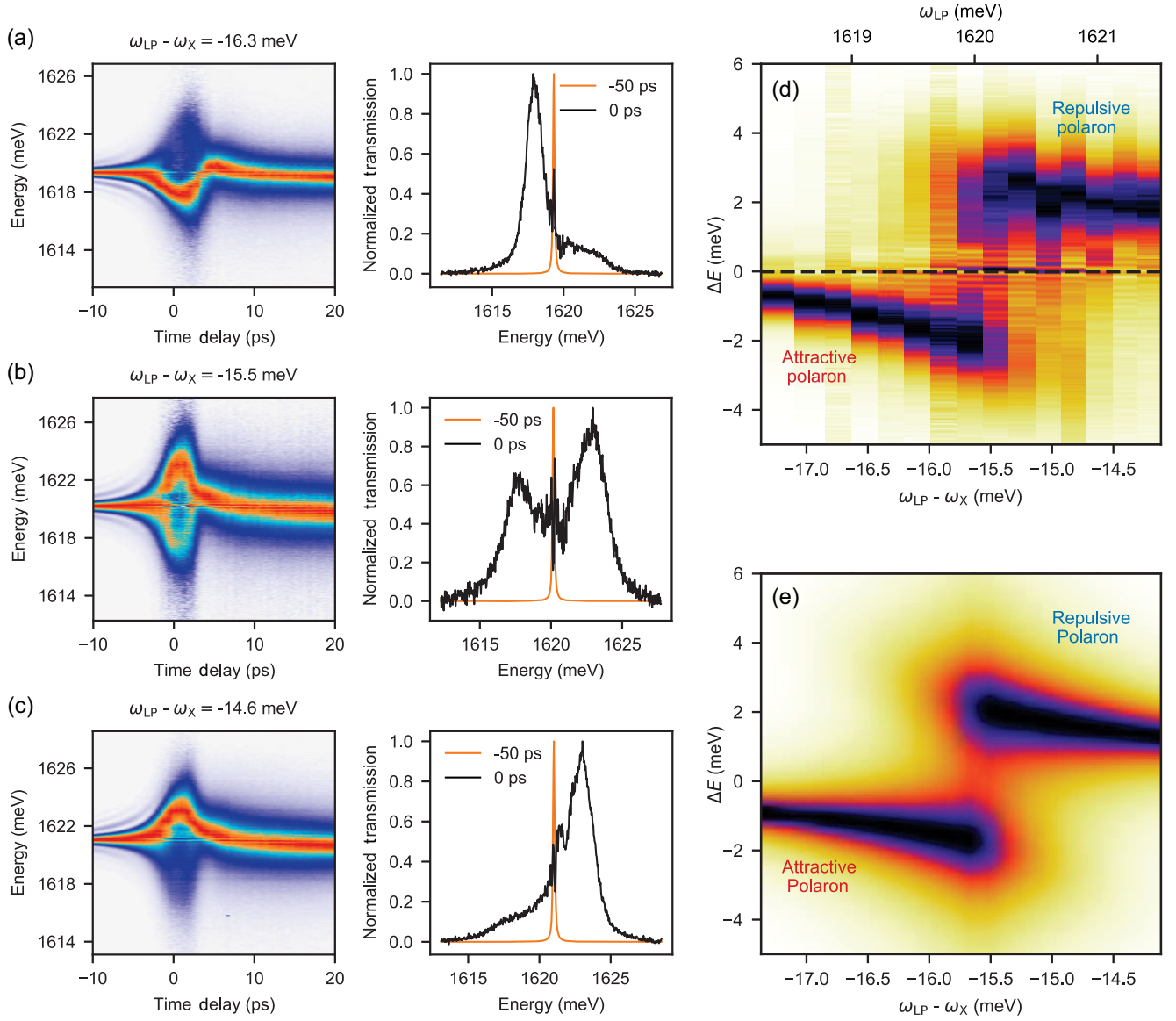


FIG. 2. (a)–(c) Left panel: Normalized probe transmission as a function of time delay for  $\omega_{\text{LP}} - \omega_{\text{X}} = -16.3$  meV,  $-15.5$  meV, and  $-14.6$  meV at an estimated bath exciton-polariton density of  $n_{\text{b}} = 6.3 \times 10^{11}$  cm $^{-2}$  and impurity density  $n_{\text{i}} = 0.15 \times 10^{11}$  cm $^{-2}$  at zero time delay, respectively. At negative time delays, i.e., before the arrival of the pump pulse that creates the bath polaritons, the transmitted probe spectrum peaks at the lower exciton-polariton energy for all detunings. Starting from  $-2$  ps towards positive time delays, the probe population has significant temporal overlap with the pumped population, which leads to the formation of Bose polarons. At resonance, where  $\omega_{\text{LP}} - \omega_{\text{X}} \approx -15.5$  meV, the attractive and repulsive branches have approximately equal weight. At red (blue) detuning, the attractive (repulsive) branch dominates. (a)–(c) Right panel: Line cuts of the normalized probe transmission spectrum at negative (orange) and zero (black) time delays. (d) Transmission spectrum as measured from the undressed exciton-polariton energy as a function of detuning at zero time delay exhibiting the attractive and repulsive polaron branches. At zero time delay, the bath density introduced by the pump pulse is estimated to be  $n_{\text{b}} = 6.3 \times 10^{11}$  cm $^{-2}$ . (e) Simulated Bose polaron spectrum with the fit parameters  $n_{\text{b,theo}} = 2.5 \times 10^{11}$  cm $^{-2}$  and  $\gamma_{\text{XX}} = 2.5$  meV.

The peak bath density is determined to be  $n_{\text{b}} = 6.3 \times 10^{11}$  cm $^{-2}$  (see the Appendix). We observe that for two-polariton energies ( $\omega_{\text{LP},\sigma^+} + \omega_{\text{LP},\sigma^-}$ ) below (above) the biexciton energy, the probe polariton resonance is shifted to lower (higher) energies, and as the energy

$\omega_{\text{LP}} - \omega_{\text{X}} \sim -15.5$  meV is approached, the two branches exhibit an avoided crossing.

To explore the physics behind our observation, we follow the theoretical framework developed in Ref. [23] to model the system by the Hamiltonian

$$\begin{aligned} \mathcal{H} = & \sum_{\mathbf{k}} \left[ \omega_X(\mathbf{k}) b_{\mathbf{k}}^\dagger b_{\mathbf{k}} + \omega_C(\mathbf{k}) c_{\mathbf{k}}^\dagger c_{\mathbf{k}} + \frac{\Omega}{2} (b_{\mathbf{k}}^\dagger c_{\mathbf{k}} + \text{H.c.}) \right. \\ & \left. + (\omega_{\text{LP}}(\mathbf{k}) - \omega_{\text{LP}}(0)) L_{\mathbf{k}}^\dagger L_{\mathbf{k}} \right] \\ & + \frac{1}{A} \sum_{\mathbf{k}, \mathbf{k}', \mathbf{q}} g_{\text{ib}}(\mathbf{k}, \mathbf{k}') L_{\mathbf{k}}^\dagger b_{\mathbf{q}-\mathbf{k}}^\dagger b_{\mathbf{q}-\mathbf{k}'} L_{\mathbf{k}'}. \end{aligned} \quad (1)$$

We recognize that due to their large binding energy in TMD, excitons can be regarded as pointlike particles at the densities of our experiment. Here, the probe excitons ( $b_{\mathbf{k}}^\dagger$ ) and photons ( $c_{\mathbf{k}}^\dagger$ ) with their respective energies  $\omega_X(\mathbf{k}) = \omega_X + \mathbf{k}^2/2m_X$  and  $\omega_C(\mathbf{k}) = \omega_X + \delta + \mathbf{k}^2/2m_C$  are coupled by the light-matter interaction  $\Omega$ . Because the pump laser is tuned to the lower polariton resonance, the rotation into the polariton basis [with respective operators  $L_{\mathbf{k}}^\dagger$  and energies  $\omega_{\text{LP}}(\mathbf{k})$ ] has already been performed for the bath excitations. The interaction between pump and probe excitons is modeled by a contact interaction of strength  $g$ , which, in the polariton basis, results in the interaction  $g_{\text{ib}}(\mathbf{k}, \mathbf{k}') = g \cos \theta_{\mathbf{k}} \cos \theta_{\mathbf{k}'}$  between pump polaritons and probe excitons. Here, the Hopfield factors  $\cos \theta_{\mathbf{k}}$  correspond to the exciton fraction in the pump polariton at momentum  $\mathbf{k}$ . The system area is denoted by  $A$ . The finite lifetimes of probe photons and pump polaritons are included in the model as phenomenological parameters (see the Appendix).

The modified polariton impurity eigenstates can be approximately described using the Ansatz [23,24]

$$\begin{aligned} |\psi\rangle &= \left( \phi^C c_0^\dagger + \phi^X b_0^\dagger + \frac{1}{\sqrt{NA}} \sum_{\mathbf{k}} \phi_{\mathbf{k}} b_{\mathbf{k}}^\dagger L_{-\mathbf{k}}^\dagger L_0 \right) |L\rangle \\ &\equiv \hat{a}^\dagger |L\rangle, \end{aligned} \quad (2)$$

where  $\phi^C$ ,  $\phi^X$ , and  $\phi_{\mathbf{k}}$  are variational parameters.

Even though approximating the wave function of the pump-induced lower polaritons with a coherent state has been successfully applied to describe pump-probe spectra in semiconductor microcavities [15,16], such an approach cannot capture nonlinear effects such as impurity-impurity interactions, whose study is the focus of our work. We instead use a variational wave-function Chevy Ansatz for the Bose polaron, where the bath is approximated by a Fock state of polaritons, which in turn enables the study of interactions between polarons. Our approach is justified since the timescales associated with the interactions are short compared to that in which bath occupancy fluctuates due to dissipation. Since the bath occupancy satisfies  $\langle n_b \rangle \gg \sqrt{\langle n_b \rangle}$ , the interaction strength is insensitive to fluctuations in  $n_b$ .

In Eq. (2), the resonant pump laser creates a coherent state of lower polaritons, which we approximate by the Fock state  $|L\rangle = (N!)^{-1/2} (L_0^\dagger)^N |0\rangle$ , which is an accurate approximation for a coherent state in the limit of large

polariton number  $N = An_{b,\text{theo}}$ . The first two terms account for the hybridization of the photon and the exciton into polaritons, while the third term reflects the dressing of the exciton by bath polaritons, leading to the formation of a polaron cloud.

Using the Ansatz (2), we calculate the transmission probe spectrum [Fig. 2(e)], using the independently measured biexciton binding energy  $\omega_{\text{XXB}}$  as input. The biexciton decay width  $\gamma_{\text{XX}}$  in turn is treated as a fit parameter due to the absence of an experimentally determined value. More importantly, we also take the peak bath density  $n_{b,\text{theo}}$  as an additional fit parameter. Using this procedure, we find a theoretical value  $n_{b,\text{theo}}$  that is smaller than the experimentally estimated value by a factor  $\beta = 2.6$ ; this difference can be attributed to the fact that the absolute value of the experimentally estimated polariton density  $n_b$  is subject to a large uncertainty. Using only the two fit parameters  $n_{b,\text{theo}}$  and  $\gamma_{\text{XX}}$ , we find remarkable agreement between theory and experiment across the full range of detunings and frequencies. This agreement gives a solid foundation to the interpretation of the observed response of the probe pulse as being due to the formation of APs and RPs, arising from the dynamical dressing of the polariton impurity by the polariton bath.

While Bose polarons exhibiting RP and AP branches have previously been observed in cold atom systems [5,7,17], our transmission data are the first evidence for their existence in 2D materials. To further characterize their properties and the role of medium dressing in this light-matter coupled system, we study the polaron spectrum measured at zero time delay and at fixed detuning  $\omega_{\text{LP}} - \omega_X = -15.5$  meV for various bath densities; see Fig. 3(a). At low densities, there is no discernible splitting between the two branches. As the bath density is increased, the finite splitting appears and grows, rendering the two peaks distinct. By fitting each spectrum with a sum of two Lorentzians, we extract the peak energies of each polaron branch [Fig. 3(b)] and their corresponding splitting  $E_{\text{split}}$  [Fig. 3(c)] as a function of the bath density.

Both the RP and AP states and their respective energies are captured by wave functions of the form in Eq. (2). The predicted splitting of these are shown as orange squares in Fig. 3(c). In this calculation, the theoretical densities are rescaled by the fixed factor  $\beta = 2.6$ , obtained from the measurement of the transmission spectrum in Fig. 2. We find that the theoretical model predicts a slight shift with density for the detuning at which the ‘‘jump’’ in the spectral weight from the attractive to the repulsive branch occurs, which was also predicted for cold atomic gases. This shift is not observed in the experiment, which may be attributed to finite range effects (that are, to a large degree, negligible in the cold atom setting) and not included in our theoretical model. Accounting for this, we extract the predicted energy splitting  $E_{\text{split}}$  for the detuning at which the transfer of weight occurs in the theoretical data. The theory is in good

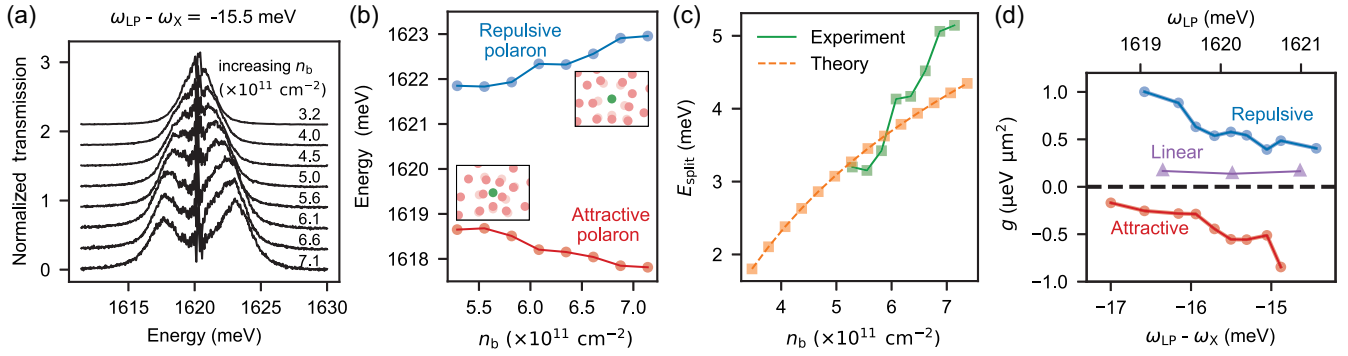


FIG. 3. (a) Normalized Bose polaron transmission spectrum for bath densities  $n_b = 3.2 \times 10^{11} \text{ cm}^{-2}$  to  $7.1 \times 10^{11} \text{ cm}^{-2}$  at  $\tau = 0 \text{ ps}$ , and impurity density  $n_i = 0.15 \times 10^{11} \text{ cm}^{-2}$ . At low bath densities, the splitting between the two branches is much smaller than their linewidths. As the bath density is increased, the attractive and repulsive branches become clearly distinguishable as the splitting grows. The spectra for different bath densities are offset for clarity. (b) Peak energies of the repulsive (attractive) branch in blue (red) circles as a function of bath density. The energies are obtained from Lorentzian fits to the measured spectrum. (c) Comparison of the measured (green) and calculated (orange) energy splittings between the attractive and the repulsive branch as a function of bath density. (d) Impurity-bath interaction strength  $g_{ib}$  of the repulsive (attractive) branch in blue (red) circles as a function of detuning. The purple triangles correspond to the polariton-polariton interaction strength [ $g_{ii}(n_b = 0)$ ] measured in linear polarization as a function of the detuning.

qualitative agreement with the experimental data. However, while we experimentally observe a linear scaling of the splitting with respect to the bath density  $n_b$ , the scaling, in theory, is sublinear. A possible source of the different scaling might again arise from finite range corrections.

For a sufficiently large bath density, we can approximate the impurity-bath interaction as a Kerr-type nonlinearity and obtain an *effective* interaction strength  $g_{ib}^{\text{eff}}$  between the impurity and bath polaritons from the gradient of the peak polaron energies with respect to the bath density:  $\Delta\omega = g_{ib}^{\text{eff}} n_b n_i$ . As shown in Fig. 3(d), by tuning across the biexciton resonance, the interaction strength varies from  $g_{ib}^{\text{eff}} = 0.4 \mu\text{eV } \mu\text{m}^2$  to  $1 \mu\text{eV } \mu\text{m}^2$  on the RP branch and from  $g_{ib}^{\text{eff}} = -0.2 \mu\text{eV } \mu\text{m}^2$  to  $-0.8 \mu\text{eV } \mu\text{m}^2$  on the AP branch. This finding implies that the magnitude of the interaction strength between opposite-spin polaritons can be enhanced by a factor of up to about 5 times in comparison to that of parallel-spin polaritons in the absence of a bath [ $g_{ii}(n_b = 0) = 0.2 \mu\text{eV } \mu\text{m}^2$ ]. Most importantly, not only the magnitude but also the sign of  $g_{ib}$  is tunable. This can be understood as a consequence of the polariton-biexciton Feshbach resonance where by tuning the energy of a scattering state across a bound state, interactions can be enhanced and their sign can be reversed [16,25,26].

#### IV. INDUCED INTERACTIONS BETWEEN BOSE POLARONS

Next, we address the question of how the interactions between two impurities are modified when they form polaronic quasiparticles due to their coupling to a bosonic bath. To this end, we now keep the bath density fixed at  $n_b = 2.6 \times 10^{11} \text{ cm}^{-2}$  and monitor the changes in the energy of the AP and RP excitations as a function of the

impurity density ranging from  $n_i = 0.15 \times 10^{11} \text{ cm}^{-2}$  to  $1.4 \times 10^{11} \text{ cm}^{-2}$ . In the top panel of Fig. 4, the polaron spectrum measured at zero time delay is shown as black lines for various impurity densities. The probe spectrum, measured at  $\tau = -50 \text{ ps}$  where the impurity is undressed [orange lines in Figs. 4(a) and 4(b)], was recorded for each probe power and serves as a control experiment. In these spectra, the residual energy shifts arise due to interactions between the impurities in the presence of the long-lived incoherent heating effects induced by the previous pump pulses (see Fig. 6 in the Appendix).

For the AP-polariton branch, we find that the energy of the dressed impurities blueshifts as their density is increased. For RP polaritons on the other hand, we find the opposite effect: Increasing the impurity density leads to a redshift, which means that increasing the density of repulsive polarons lowers the energy to create further repulsive polarons. By taking the gradient of the energy shifts with respect to the impurity density, we can extract the effective interaction strength between the polaron-polaritons [see Figs. 4(c) and 4(d)]. For APs, this leads to a repulsive interaction strength  $g_{ii} = 0.12 \mu\text{eV } \mu\text{m}^2$  while RP polaritons experience an attractive interaction strength of  $g_{ii} = -0.11 \mu\text{eV } \mu\text{m}^2$ . These interaction values have been measured relative to the polariton-polariton interaction strength without bath interactions  $g_{ii}(n_b = 0) = 0.2 \mu\text{eV } \mu\text{m}^2$  [see purple data in Fig. 3(d)].

We repeat this procedure for other pump densities ( $n_b = 4.0$  and  $6.3 \times 10^{11} \text{ cm}^{-2}$ ) and extract values for the impurity-impurity interactions  $g_{ii}(n_b)$  as a function of the bath density, which we plot in Fig. 4(e) for the AP (red) and RP (blue) polaritons. For AP polaritons, the interactions become more repulsive upon increasing the bath density. In contrast, for the RP polaritons, the dressing

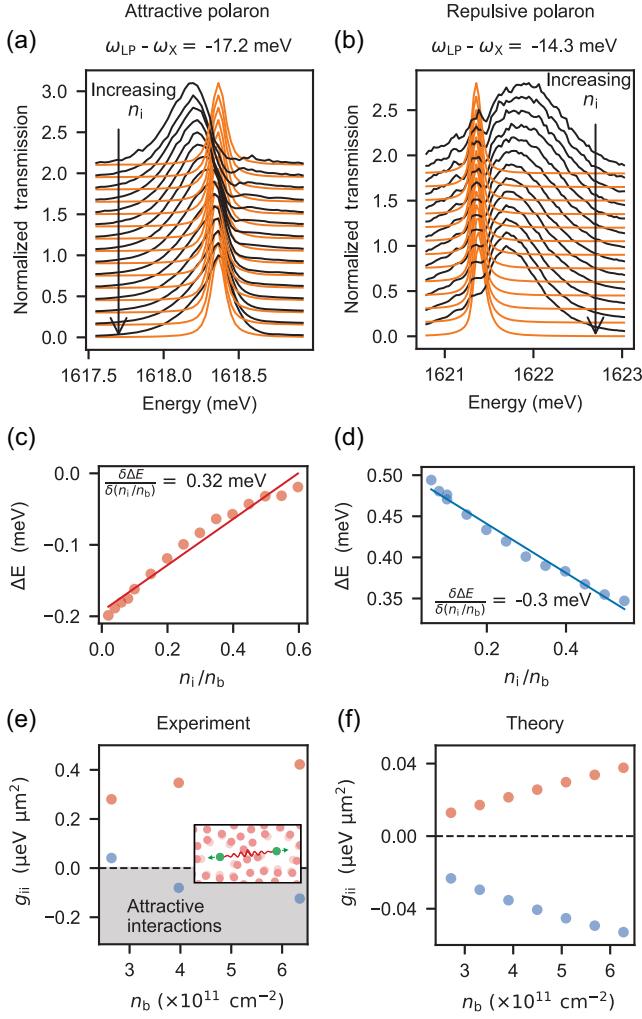


FIG. 4. Top panel: Normalized impurity density-dependent polaron [(a) attractive and (b) repulsive] spectrum in black lines ( $\tau = 0$  ps) and the corresponding undressed exciton-polariton spectrum (measured at  $\tau = -50$  ps) in orange lines. The bath density is  $n_b = 2.6 \times 10^{11} \text{ cm}^{-2}$ . The spectra for different impurity densities are plotted with an offset for clarity. Middle panel: Impurity-impurity interaction shift of the repulsive (c) and attractive (d) branches as a function of the ratio between impurity and bath density, at  $n_b = 2.6 \times 10^{11} \text{ cm}^{-2}$ . Bottom panel: Experimentally (e) and theoretically (f) obtained impurity-impurity interaction strengths as a function of the bath density. In both cases, the values for the attractive (repulsive) polaron are given by the red (blue) dots. The interaction strength has been measured with respect to the undressed polariton spectrum, which includes polariton-polariton interactions in the same valley, implying that the interaction strength values above the gray shaded area are repulsive. The inset in panel (e) symbolizes the repulsive interactions between impurities (green dots) repulsively dressed by excitations of bath particles (red dots).

from increasing the density of bath particles leads to a reduction of the polaron interactions compared to the bare repulsive polariton interactions. For the largest bath density that is experimentally achievable, we even find that the

interactions between RP polaritons become attractive. This observation demonstrates that by polaron dressing, one can not only strongly modify the magnitude of polariton interactions but even change their sign and turn repulsive interactions between bare impurity particles into net attractive interactions upon Bose polaron formation.

To theoretically investigate the interaction between polarons, we compute the expectation value of the Hamiltonian (1) with respect to a two-polaron state

$$E^{2\text{Pol}} = \frac{\langle \mathbf{L} | \hat{a} \hat{a} \mathcal{H} \hat{a}^\dagger \hat{a}^\dagger | \mathbf{L} \rangle}{\langle \mathbf{L} | \hat{a} \hat{a} \hat{a}^\dagger \hat{a}^\dagger | \mathbf{L} \rangle}. \quad (3)$$

In this first-order model, the correlations between the polarons are neglected on the level of the wave function (up to the normalization). The dependence of  $E^{2\text{Pol}}$  on the probe exciton density is extracted by varying the system area at fixed pump polariton density  $n_{b,\text{theo}} = N/A$ . From the dependence of the attractive and repulsive polaron energy on the ratio between probe and pump densities  $n_i/n_b$ , we extract the effective interaction strength of the polaron-polaritons, which is shown in Fig. 4(f) as a function of the bath density. Remarkably, already within the simple Ansatz (3), the same qualitative behavior of the energy shift as the one observed in the experiment is obtained. However, the extracted effective interaction strengths differ by a factor 5 for the RPs, and by a factor 10 for the APs, which we attribute to the uncertainty of the polariton density, the simplified Chevy-Ansatz-based model used for the calculation of polaron-polaron interactions, as well as the modeling of the impurity density as arising from a simple finite-size effect.

## V. CONCLUSION

The experimental realization of Bose polarons enables tunable polariton interactions in both magnitude and sign; this should be contrasted with polariton interactions in the absence of a bath, which are repulsive and weak. Our results present an important step towards the study of interactions in nonequilibrium polaronic systems, which can guide further theoretical and experimental studies of novel quantum states of matter ranging from bipolarons [9,27–29] to induced superconductivity [30,31]. For the case of bosonic, mobile impurities, our experiment demonstrates that polaron effects can turn repulsive interactions into attractive ones. Applying the observed Bose polaron effects to an electronic system may thus allow us to weaken or even overcome the Coulomb repulsion between electrons [32], opening up avenues for identifying new unconventional mechanisms of electron pairing in van der Waals materials based on exciton or polariton exchange.

The data are available at the ETH Research Collection [33].



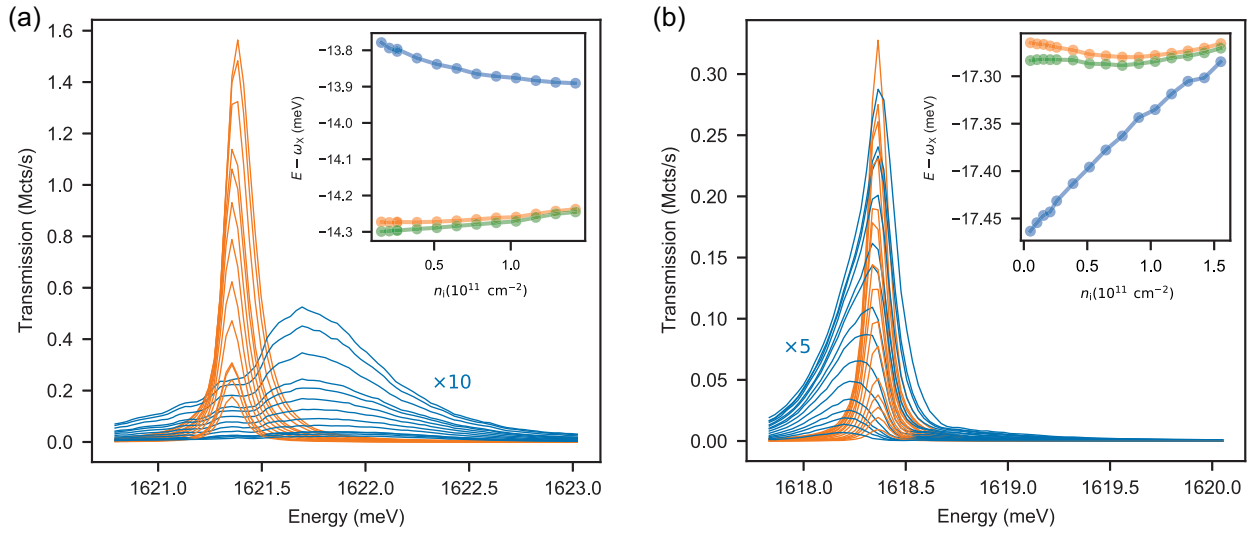


FIG. 6. Impurity-density-dependent transmission spectra, as in Figs. 4(a) and 4(b) but not normalized, for the attractive and repulsive polaron in panels (a) and (b), respectively. The blue lines correspond to the polaron spectrum at  $\tau = 0$  ps. The data are multiplied by the indicated factor for clarity. The orange lines represent the reference transmission spectra of the probe laser at  $\tau = -50$  ps. The insets show the extracted resonance energies of the probe laser transmission spectra as a function of the impurity density  $n_i$ . The blue dots are obtained from fitting the polaron spectrum (at  $\tau = 0$  ps), the orange dots from the reference spectrum ( $\tau = -50$  ps), and the green dots from the probe laser transmission spectrum with the pump laser blocked from reaching the sample. The resonance energies are plotted with respect to the exciton energy  $\omega_X$ .

FWHM of less than or equal to 0.5 meV using a  $4f$  pulse shaper while the probe pulses are precompensated for dispersion using a four-pass, free-space, single grating pulse compressor setup. The time delay  $\tau$  between the pump and the probe pulses is controlled with a delay stage. The pump and the probe pulses are then sent through individual optical fibers to the dipstick for measurement. At the sample position, the pump and probe pulses are measured to be 3 ps and 200 fs in duration, respectively. The optical excitation is done via the free-space access to the cavity, which allows for individually controlling their respective polarization, while the transmission signal is collected from the fiber access of the cavity. The transmission signal is polarization filtered to suppress the transmitted pump signal from reaching the detector. The signal is measured using a spectrometer with a grating of 1500 grooves per mm and a liquid-nitrogen-cooled CCD camera.

In order to estimate the polariton density, we measure the incident pump power  $P_{\text{pump}}$  in the free-space path just before the entrance window into the dipstick. The effective pump power that excites the system is  $\epsilon\eta P_{\text{pump}}$ , where  $\epsilon$  is the spectral overlap of the pump and the polariton mode and  $\eta$  is the spatial overlap of the pump mode and the cavity mode. Note that  $\epsilon$  is determined from the pump laser spectrum and the transmitted polariton spectrum while  $\eta$  is determined from the signal reflected from the cavity upon white light excitation. The number of photons per pulse can be determined as  $N_{\text{pulse}} = (\epsilon\eta P_{\text{pump}} / \hbar\omega f_{\text{rep}})$ , where  $f_{\text{rep}} = 76$  MHz is the repetition rate of the pulsed laser. This

corresponds to the integral under the temporal profile of the pump pulse. The time evolution of the polariton number in the system can then be obtained by convolving the exponential response function of the polariton with the pump temporal profile.

## 2. Theory

We include a finite lifetime for the probe photon and the pump polariton by adding an imaginary part to the single-particle energies in Eq. (1), i.e.,  $\omega_C(\mathbf{k}) \rightarrow \omega_C(\mathbf{k}) - i\gamma_C$ ,  $\omega_{\text{LP}}(\mathbf{k}) \rightarrow \omega_{\text{LP}}(\mathbf{k}) - i\gamma_{\text{LP}}$ , with  $\gamma_C$  the inverse lifetimes of the probe photon. The inverse lifetime of the pump polariton is given by  $\gamma_{\text{LP}} = -(1 - \cos^2 \theta_0)\gamma_C$ , where

$$\cos \theta_{\mathbf{k}} = \frac{1}{\sqrt{2}} \sqrt{1 + \frac{|\omega_C(\mathbf{k}) - \omega_X(\mathbf{k})|}{\sqrt{(\omega_C(\mathbf{k}) - \omega_X(\mathbf{k}))^2 + \Omega^2}}} \quad (\text{A1})$$

is the Hopfield factor. We do not consider a finite lifetime for the probe exciton in order to reduce the number of fit parameters.

The linear transmission probe spectrum is related to the impurity Green's function by  $\mathcal{T}(\mathbf{k}, E) = |\mathbf{G}_{22}(\mathbf{k}, E)|^2$ , which, in the exciton-photon basis, reads

$$\mathbf{G}(E) = \begin{pmatrix} \omega_X(0) - E + \Sigma(E) & \frac{\Omega}{2} \\ \frac{\Omega}{2} & \omega_C(0) - i\gamma_C - E \end{pmatrix}^{-1}. \quad (\text{A2})$$

Within our Ansatz, the self-energy takes the form  $\Sigma(E) = \cos^2\theta_0 n_b / (g^{-1} + A^{-1} \sum_{\mathbf{k}} \cos^2\theta_{\mathbf{k}} / \xi_{\mathbf{k}})$  with  $\xi_{\mathbf{k}} = \omega_{\mathbf{X}}(\mathbf{k}) + (\omega_{\text{LP}}(\mathbf{k}) - \omega_{\text{LP}}(0)) - i\gamma_{\text{LP}} - E$ . Since any purely attractive, short-range interaction supports a bound state in 2D, the interaction parameter  $g$  can be related to the binding energy  $\omega_{\text{XXB}}$  and inverse lifetime  $\gamma_{\text{XX}}$  of the biexciton via  $-1/g = A^{-1} \sum_{\mathbf{k}} 1/(\omega_{\text{XXB}} - i\gamma_{\text{XX}} + 2\omega_{\mathbf{X}}(\mathbf{k}))$ . For the spectrum shown in Fig. 2, we used the experimental values  $\Omega = 15$  meV,  $\gamma_{\text{C}} = 0.1$  meV,  $\omega_{\text{XXB}} = 29.35$  meV, and  $\omega_{\text{LP}}(0) - \omega_{\mathbf{X}}(0) = -15.5$  meV, and obtained  $\gamma_{\text{XX}} = 2.5$  meV and  $n_b = 2.5 \times 10^{11}$  cm<sup>-2</sup> from fitting the experimental data.

For the calculation of the two-polaron energy  $E^{2\text{Pol}}$ , we evaluate Eq. (3) using the variational parameters obtained from minimizing the energy functional for the single polaron state. Note that the Hamiltonian itself does not contain an interaction between impurities: The probe excitons exclusively interact through the presence of a bath. It is therefore crucial to work with a fixed particle number of pump polaritons in the Ansatz (2).

- 
- [1] A. Schirotzek, C.-H. Wu, A. Sommer, and M. W. Zwierlein, *Observation of Fermi Polarons in a Tunable Fermi Liquid of Ultracold Atoms*, *Phys. Rev. Lett.* **102**, 230402 (2009).
- [2] S. Nascimbène, N. Navon, K. J. Jiang, L. Tarruell, M. Teichmann, J. McKeever, F. Chevy, and C. Salomon, *Collective Oscillations of an Imbalanced Fermi Gas: Axial Compression Modes and Polaron Effective Mass*, *Phys. Rev. Lett.* **103**, 170402 (2009).
- [3] C. Kohstall, M. Zaccanti, M. Jag, A. Trenkwalder, P. Massignan, G. M. Bruun, F. Schreck, and R. Grimm, *Metastability and Coherence of Repulsive Polarons in a Strongly Interacting Fermi Mixture*, *Nature (London)* **485**, 615 (2012).
- [4] M. Koschorreck, D. Pertot, E. Vogt, B. Fröhlich, M. Feld, and M. Köhl, *Attractive and Repulsive Fermi Polarons in Two Dimensions*, *Nature (London)* **485**, 619 (2012).
- [5] M.-G. Hu, M. J. Van de Graaff, D. Kedar, J. P. Corson, E. A. Cornell, and D. S. Jin, *Bose Polarons in the Strongly Interacting Regime*, *Phys. Rev. Lett.* **117**, 055301 (2016).
- [6] F. Scazza, G. Valtolina, P. Massignan, A. Recati, A. Amico, A. Burchianti, C. Fort, M. Inguscio, M. Zaccanti, and G. Roati, *Repulsive Fermi Polarons in a Resonant Mixture of Ultracold <sup>6</sup>Li Atoms*, *Phys. Rev. Lett.* **118**, 083602 (2017).
- [7] Z. Z. Yan, Y. Ni, C. Robens, and M. W. Zwierlein, *Bose Polarons Near Quantum Criticality*, *Science* **368**, 190 (2020).
- [8] M. Sidler, P. Back, O. Cotlet, A. Srivastava, T. Fink, M. Kroner, E. Demler, and A. İmamoğlu, *Fermi Polaron-Polaritons in Charge-Tunable Atomically Thin Semiconductors*, *Nat. Phys.* **13**, 255 (2016).
- [9] A. Camacho-Guardian and Georg M. Bruun, *Landau Effective Interaction between Quasiparticles in a Bose-Einstein Condensate*, *Phys. Rev. X* **8**, 031042 (2018).
- [10] S. I. Mistakidis, G. C. Katsimiga, G. M. Koutentakis, and P. Schmelcher, *Repulsive Fermi Polarons and Their Induced Interactions in Binary Mixtures of Ultracold Atoms*, *New J. Phys.* **21**, 043032 (2019).
- [11] L. B. Tan, O. Cotlet, A. Bergschneider, R. Schmidt, P. Back, Y. Shimazaki, M. Kroner, and A. İmamoğlu, *Interacting Polaron-Polaritons*, *Phys. Rev. X* **10**, 021011 (2020).
- [12] J. B. Muir, J. Levinsen, S. K. Earl, M. A. Conway, J. H. Cole, M. Wurdack, R. Mishra, D. J. Ing, E. Estrecho, Y. Lu, D. K. Efimkin, J. O. Tollerud, E. A. Ostrovskaya, M. M. Parish, and J. A. Davis, *Interactions between Fermi Polarons in Monolayer WS<sub>2</sub>*, *Nat. Commun.* **13**, 6164 (2022).
- [13] U. Neukirch, S. R. Bolton, N. A. Fromer, L. J. Sham, and D. S. Chemla, *Polariton-Biexciton Transitions in a Semiconductor Microcavity*, *Phys. Rev. Lett.* **84**, 2215 (2000).
- [14] A. I. Tartakovskii, D. N. Krizhanovskii, and V. D. Kulakovskii, *Polariton-Polariton Scattering in Semiconductor Microcavities: Distinctive Features and Similarities to the Three-Dimensional Case*, *Phys. Rev. B* **62**, R13298 (2000).
- [15] M. Saba, F. Quochi, C. Ciuti, U. Oesterle, J. L. Staehli, B. Deveaud, G. Bongiovanni, and A. Mura, *Crossover from Exciton to Biexciton Polaritons in Semiconductor Microcavities*, *Phys. Rev. Lett.* **85**, 385 (2000).
- [16] N. Takemura, S. Trebaol, M. Wouters, M. T. Portella-Oberli, and B. Deveaud, *Polaritonic Feshbach Resonance*, *Nat. Phys.* **10**, 500 (2014).
- [17] N. B. Jørgensen, L. Wacker, K. T. Skalmstang, M. M. Parish, J. Levinsen, R. S. Christensen, G. M. Bruun, and J. J. Arlt, *Observation of Attractive and Repulsive Polarons in a Bose-Einstein Condensate*, *Phys. Rev. Lett.* **117**, 055302 (2016).
- [18] I. Carusotto and C. Ciuti, *Quantum Fluids of Light*, *Rev. Mod. Phys.* **85**, 299 (2013).
- [19] K. Hao, J. F. Specht, P. Nagler, L. Xu, K. Tran, A. Singh, C. K. Dass, C. Schüller, T. Korn, M. Richter, A. Knorr, X. Li, and G. Moody, *Neutral and Charged Inter-Valley Biexcitons in Monolayer MoSe<sub>2</sub>*, *Nat. Commun.* **8**, 15552 (2017).
- [20] Takahiro Uto, Bertrand Evrard, Kenji Watanabe, Takashi Taniguchi, Martin Kroner, and Atac İmamoğlu, *Interaction Induced ac-Stark Shift of Exciton-Polaron Resonances*, *arXiv:2306.01778*.
- [21] This observation implies a biexciton binding energy larger than what has been reported in earlier experiments, which yielded  $\omega_{\text{XXB}} = 20$  meV [19,22], and it is not consistent with our findings.
- [22] C.-K. Yong, J. Horng, Y. Shen, H. Cai, A. Wang, C.-S. Yang, C.-K. Lin, S. Zhao, K. Watanabe, T. Taniguchi, S. Tongay, and F. Wang, *Biexcitonic Optical Stark Effects in Monolayer Molybdenum Diselenide*, *Nat. Phys.* **14**, 1092 (2018).
- [23] J. Levinsen, F. M. Marchetti, J. Keeling, and M. M. Parish, *Spectroscopic Signatures of Quantum Many-Body Correlations in Polariton Microcavities*, *Phys. Rev. Lett.* **123**, 266401 (2019).
- [24] M. A. Bastarrachea-Magnani, A. Camacho-Guardian, M. Wouters, and G. M. Bruun, *Strong Interactions and Biexcitons in a Polariton Mixture*, *Phys. Rev. B* **100**, 195301 (2019).

- [25] M. Wouters, *Resonant Polariton-Polariton Scattering in Semiconductor Microcavities*, *Phys. Rev. B* **76**, 045319 (2007).
- [26] I. Carusotto, T. Volz, and A. İmamoğlu, *Feshbach Blockade: Single-Photon Nonlinear Optics Using Resonantly Enhanced Cavity Polariton Scattering from Biexciton States*, *Europhys. Lett.* **90**, 37001 (2010).
- [27] A. S. Alexandrov and A. B. Krebs, *Polarons in High-Temperature Superconductors*, *Sov. Phys. Usp.* **35**, 345 (1992).
- [28] A. S. Alexandrov and N. F. Mott, *Bipolarons*, *Rep. Prog. Phys.* **57**, 1197 (1994).
- [29] A. Camacho-Guardian, L. A. Peña Ardila, T. Pohl, and G. M. Bruun, *Bipolarons in a Bose-Einstein Condensate*, *Phys. Rev. Lett.* **121**, 013401 (2018).
- [30] F. P. Laussy, A. V. Kavokin, and I. A. Shelykh, *Exciton-Polariton Mediated Superconductivity*, *Phys. Rev. Lett.* **104**, 106402 (2010).
- [31] O. Coteř, S. Zeytinođlu, M. Sigrist, E. Demler, and A. İmamođlu, *Superconductivity and Other Collective Phenomena in a Hybrid Bose-Fermi Mixture Formed by a Polariton Condensate and an Electron System in Two Dimensions*, *Phys. Rev. B* **93**, 054510 (2016).
- [32] Ruipeng Li, Jonas von Milczewski, Atac Imamoglu, Rafal Oldziejewski, and Richard Schmidt, *Impurity-Induced Pairing in Two-Dimensional Fermi Gases*, *Phys. Rev. B* **107**, 155135 (2023).
- [33] M. Kroner, <http://hdl.handle.net/20.500.11850/586847>.